Top Catal (2013) 56:1716–1723
DOI 10.1007/s11244-013-0107-1

ORIGINAL PAPER

Microchannel Autothermal Reforming of Methane to Synthesis Gas

Mustafa Karakaya · Z. Ilsen Onsan · Ahmet K. Avci

Published online: 27 June 2013

Abstract Autothermal reforming of methane to synthesis gas (CO and H_2) is studied in a microchannel reactor comprised of Pt- and Rh-based catalysts that are coated on opposite walls of the channel. The effects of operating parameters and microchannel catalyst configuration on methane conversion and CO selectivity are analyzed. The parameters considered are the residence time of the reactants (12.9–25.7 ms), reaction temperature (500–650 °C), molar steam-to-carbon (S/C = 0–3.0) and oxygen-to-carbon (O_2/C = 0.47–0.63) ratios at the inlet. Doubling the residence time leads to ca. 10 % increase in methane conversion, but has only a 4 % contribution to the CO selectivity. Higher O_2/C ratios improve extent of methane oxidation, but reduce selectivity due to CO_2 production. When the temperature is raised from 500 to 650 °C, conversion increases from 12.8 to 46.6 % and selectivity increases from 20.1 to 35.7 %. S/C ratio has the greatest effect on the outlet H_2/CO ratio, which is found to vary between 0.93 and 2.68, via the water–gas shift reaction. Comparison of the present catalyst configuration with the use of bimetallic Pt–Rh coating in the microchannel under identical conditions shows that the latter can improve conversion by 20 % and CO selectivity by 33 %.

Keywords Autothermal reforming · Methane · Microchannel reactor · Synthesis gas · Wall-coated catalyst

M. Karakaya · Z. Ilsen Onsan · A. K. Avci (✉)
Department of Chemical Engineering, Bogazici University, Bebek 34342, Istanbul, Turkey
e-mail: avciahme@boun.edu.tr

Present Address:
M. Karakaya
R&D Department, Turkish Petroleum Refineries. Co, Korfez 41790, Kocaeli, Turkey

1 Introduction

Synthesis gas is an important feedstock in chemicals production processes such as Fischer–Tropsch (FT), methanol and dimethyl ether (DME) syntheses. Autothermal reforming (ATR) of natural gas is the well-established industrial practice of producing syngas, which involves the spatial integration of exothermic partial oxidation (POX) and endothermic steam reforming (SR) of the fuel that is co-fed into the reactor with steam and oxygen. Due to the immediate and effective supply of heat from the oxidation to the reforming reactions, external heating requirements are minimal [1–4]. ATR of methane, model fuel for natural gas, is carried out over Ni-based catalysts at temperatures in excess of 900 °C in order to affect the syngas feed ratio in favor of the FT ($2.0 < H_2/CO < 2.2$) or methanol ($H_2/CO \approx 3.0$) syntheses [5]. Problems associated with ATR over Ni include deactivation and loss of reforming activity of the catalysts by oxidation [6], hot spot formation at the reactor upstream due to very high oxidation rates [7], and carbon deposition on the catalysts [8]. Hot spots during ATR can be suppressed by utilizing Pt- [9] and Rh-based [10] catalysts. Moreover, along with Pt and Rh, other noble metals (Ru and Ir) exhibit prominently higher SR activity [11], and are much less prone to carbon deposition [12]. Even though Ni-based catalysts are used in large-scale production of syngas owing to their availability and low costs, use of noble metals may sometimes be viable due to their superior activity, selectivity, and stability under harsh operating conditions [13].

The use of catalytic microchannel reactors has been proposed to offer potential solutions to problems such as those mentioned above and additional benefit of increase in productivity per unit volume or mass of catalyst [13, 14]. With characteristic dimensions less than 1×10^{-3} m, microchannel reactors allow for high surface area-to-volume ratios

and enhanced heat transfer coefficients that are one or two orders of magnitude greater than those in conventional tubular reactors [14–18]. This facilitates rapid delivery of the released heat throughout the microchannel and across the metallic channel walls, thus quenching the highly exothermic oxidation reactions and inhibiting local hot spots [19–21]. Moreover, since excessive pressure drop along the channels is not a concern, it is possible to operate at millisecond level residence times, which can be manipulated so as to suppress undesired slow reactions leading to coke formation [22, 23]. In view of these aspects, POX of methane in microchannel or structured reactors has been studied over different metal-based catalysts. Fichtner et al. [24] used a honeycomb catalyst made of Rh foils whose high thermal conductivity provided a good heat distribution in the flow direction that led to higher methane conversions and CO selectivities. Younes-Metzler et al. [25] demonstrated that POX of methane could be carried out over a Pd-based catalyst within safety margins due to good reaction control. Enger et al. [26] tested FeCralloy and Nicrofer as the material of construction of the Rh-impregnated microchannels in terms of stability and catalytic activity, and found out that the former resulted in a thin but stable layer of alumina that increased the effective reactor surface area and provided more sites for the Rh particles. Makarshin et al. [27] compared two flow configurations, namely, co-current and counter-current flows. The latter outperformed the co-current configuration both in methane conversion and CO selectivity, especially at high heat loads, because it tended to spread out the heat over a wider catalytically active region. As for ATR of fuels other than methane, ATR of *i*-octane over Pt [28], of methanol over Pd–Zn [29], and of ethanol over Rh [30] have been studied in microchannel reactors. The issue of carbon deposition over the microchannel catalysts during SR of methane has also been addressed in several works [13, 31–34] in which the operational resistance of the catalysts has been demonstrated even at very low S/C ratios.

The present work involves experimental investigation of methane ATR in a microchannel reactor involving coated Pt and Rh catalysts under a wide range of parameters including residence time of the reactants, reaction temperature, and molar S/C as well as O_2/C ratios at the inlet. In addition to these operating parameters, the impact of microchannel catalyst configuration on methane conversion and CO selectivity is also explored.

2 Experimental

2.1 Catalyst Synthesis

The experiments are conducted over a combination of 0.2 wt% Pt/δ-Al_2O_3 and 2 wt% Rh/δ-Al_2O_3 catalysts prepared by the incipient-to-wetness impregnation method. Alumina powder of 3×10^{-6} m size (Merck, 120–190 m^2/g, γ-phase) to be used as the catalyst support is dried at 200 °C for 2 h and calcined at 900 °C for 4 h in order to transform it into the thermally stable δ-phase [35]. Calculated amounts of aqueous solutions of the Pt and Rh precursors, $[Pt(NH_3)_4](NO_3)_2$ and $Rh(NO_3)_3$ (Sigma–Aldrich) respectively, are impregnated under vacuum onto the δ-Al_2O_3 supports. After the slurries are dried overnight at 120 °C, they are calcined at 500 °C for 3 h.

Several mechanical and chemical treatment methods are required for the preparation of the catalytic microchannel. The first of these is wire electrodischarge machining of FeCrAl sheets (Goodfellow Cambridge Limited) into $2 \times 10^{-3} \times 5 \times 10^{-3} \times 2 \times 10^{-2}$ m^3 plates, and of 310-grade stainless steel into a cylindrical housing (diameter $= 18.6 \times 10^{-3}$ m, length $= 3 \times 10^{-2}$ m) shown in Fig. 1a. As a next step, in order to enhance adhesion of the coated catalysts, a native alumina layer on the plates are formed by calcining them in air at 900 °C for 2 h [13]. Then, the calcined 3×10^{-6} m catalyst powders are mixed with deionized water at a water-to-powder weight ratio of 6:1. The resulting slurries are blade-coated repeatedly onto the $5 \times 10^{-3} \times 2 \times 10^{-2}$ m^2 plates until the weight per surface area reaches ca. 200 g_{cat}/m^2. The coated plates are dried overnight at 120 °C and calcined for 3 h at 500 °C. The catalytic microchannel is finally obtained by insertion of a Pt- and Rh-coated plate into the cylindrical housing such that they face each other (Fig. 1a, b). The plates are inserted with 5×10^{-4} m fitting to the grooves at each side to give a single microchannel with dimensions $H = 7.5 \times 10^{-4}$ m, $W = 4 \times 10^{-3}$ m and $L = 2 \times 10^{-2}$ m. The height (H) includes the total thickness of the coated catalyst layers (Fig. 1a, b), with each layer being 1×10^{-4} m thick [13]. The net catalyst weights, 10.4×10^{-3} g of 2 % Rh/δ-Al_2O_3 and 15.2×10^{-3} g of 0.2 % Pt/δ-Al_2O_3, are determined after insertion of the plates into the housing and then removing them since the grooves strip off some coating on the sides during insertion. Possible displacement of the plate is prevented by packing ceramic wool into the remaining 1×10^{-2} m gap between the bottom of the catalytic plate and the bottom of the housing.

2.2 Reaction Tests

Schematic of the microchannel reactor used in the reaction tests is shown in Fig. 1c. The housing, including the catalytic Pt and Rh plates, is placed into the center of a 2×10^{-2} m (internal diameter) $\times$ 8×10^{-1} m (length) quartz tube, which is then mounted into a temperature controlled furnace such that the catalytic microchannel remains within the center of 1×10^{-1} m long constant-temperature zone. As depicted in Fig. 1c, the steel housing

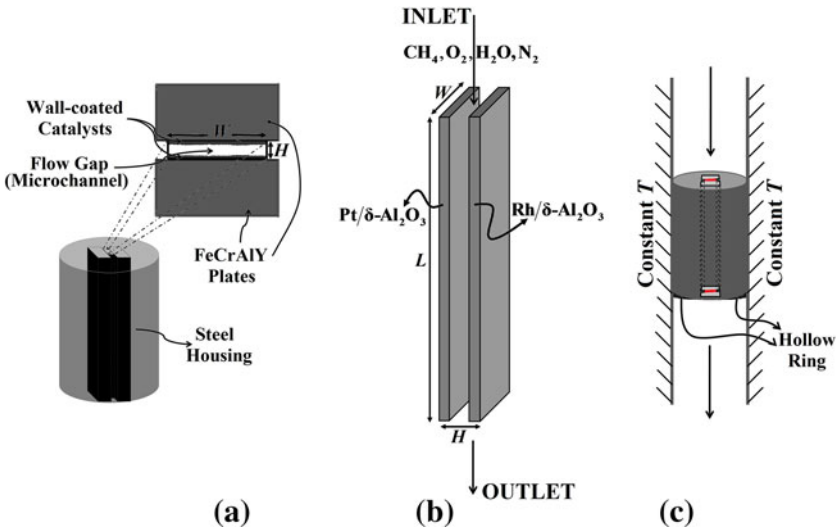

Fig. 1 **a** Orthographic drawing of the steel housing and the microchannel [34], **b** details of the microchannel configuration, **c** the microchannel reactor arrangement inside the quartz tube [34]

is supported underneath by a hollow ring that is wide enough to ensure sufficient circumferential overlap. The designed overlap keeps the housing fixed in position and prevents bypass through the annulus between the housing and the tube. The possibility of bypass is further diminished during the experiments due to the thermal expansion of the steel housing at high temperatures (>500 °C) that minimizes the annular gap. This statement is based on the fact that the housing, which can easily be placed into the quartz tube before the experiments, does not move at all upon dismantling of the tube from the furnace just after the experiments. Temperature of the catalytic zone is controlled and measured to ±0.1 K by a Shimaden FP-23 programmable temperature controller and a K-type sheathed thermocouple, which measures the skin temperature of the quartz tube from the spot that corresponds to the mid-point (i.e. point of $L = 1 \times 10^{-2}$ m (Fig. 1b)) of the catalytic microchannel.

The experiments are carried out in the following parameter ranges: (a) residence time between 12.9 ms ($v_{MC} = 210$ Nml min^{-1}) and 25.7 ms (105 Nml min^{-1}), (b) reaction temperature between 500 and 650 °C, (c) S/C ratio between 0 and 3.0, and (d) O_2/C ratio between 0.47 and 0.63. Residence time is defined as the entire flow-by volume (gap + coating volume) divided by the total volumetric flow rate (v_{MC}) at normal conditions of 298 K and 1 atm. S/C and O_2/C ratios are respectively defined as the molar ratios of steam and molecular oxygen to methane at the inlet. Before the reaction tests are initiated, the Pt and Rh catalysts are reduced in situ under 40 Nml min^{-1} H_2 flow at 800 °C for 2 h. Flow rates of the gases (H_2, CH_4, N_2, dry air) are measured and controlled by Bronkhorst F-201CV series digital thermal mass flow controllers. Shimadzu LC-20AD HPLC pump is used to feed the system with constant and pulse-free flow of deionized water, which is vaporized before mixing with other gases. A temperature-controlled electric heat tracing system is applied to all piping which is also insulated by ceramic wool to prevent condensation of water. Mole fraction of inlet methane is kept constant at 0.143 in all parametric analyses. The feed gas composition of 2.12/6.36/1.00/5.36 ($CH_4/H_2O/O_2/N_2$) is preserved at each residence time change. The S/C or O_2/C ratio is adjusted by varying the N_2 flow rate such that all other parameters (i.e., O_2/C or S/C and residence time) and the partial pressure of methane remain unchanged. Analyses that involve the parametric variations of temperature, S/C and O_2/C ratios are done only at the lowest residence time of 12.9 ms (total flow rate of 210 Nml min^{-1}). The matrix shown in Table 1 summarizes this experimental program.

Although ATR reactors can involve temperature changes, the operating parameters and the reaction system described above are customized to investigate product distribution at isothermal conditions. Flow rates are kept high enough and the feed mixture is diluted with N_2 to sweep out generated heat from the microchannel. Moreover, the reactor system is not adiabatic, and the generated heat is released from the catalytic microchannel to the outside of the quartz tube quickly via conduction through FeCrAl plate and the steel housing which are in close contact with each other (Fig. 1). Considering these together with the facts that the wall thickness of the quartz tube is 2×10^{-3} m, that the annular gap between the steel housing and the quartz tube is nearly closed at the reaction temperatures, and that the microchannel is placed within a metallic block, it can be stated that the temperature difference between the channel and the skin of the quartz tube where the thermocouple tip is located, is minimal.

Feed gas and product analyses are conducted using a Shimadzu GC-2014 gas chromatograph (GC) equipped with a Carboxen 1000 packed column and a thermal conductivity detector. Operating conditions of the GC and the methods are presented elsewhere [13]. Research-grade

Table 1 Methane ATR operating conditions in the microchannel reactor

RT (ms)	S/C							O_2/C			*T* (°C)			
	0	0.5	1.0	1.5	2.0	2.5	3.0[a]	0.47[a]	0.54	0.63	500	550	600	650[a]
12.9	×	×	×	×	×	×	×[b]	×[b]	×	×	×	×	×	×[b]
14.8							×	×						×
19.3							×	×						×
25.7							×	×						×

[a] Marked columns denote identical runs with S/C = 3.0, O_2/C = 0.47 and *T* = 650 °C

[b] Base-case values with *RT* = 12.9 ms, S/C = 3.0, O_2/C = 0.47 and *T* = 650 °C

gases of high purity (CH_4, N_2, H_2, Ar > 99.99 %, all supplied by Linde) are used in the reaction tests and GC analyses. Carbon balance between the reactant methane and the gaseous products CO and CO_2 gives the methane conversion (X_{CH_4}), Eq. (1), which is also calculated by the percent difference between inlet and outlet molar flow rate of methane, Eq. (2):

$$X_{CH_4} = 100 \times \frac{y_{CO} + y_{CO_2}}{y_{CO} + y_{CO_2} + y_{CH_4}} \quad (1)$$

$$X_{CH_4} = 100 \times \frac{F^{in}_{CH_4} - F^{out}_{CH_4}}{F^{in}_{CH_4}} \quad (2)$$

Eq. (1) is based on a carbon balance, and assumes that the carbon in the converted methane exists in CO and CO_2, and no solid carbon is generated as a product. Therefore, when the conversions calculated from Eqs. (1) and (2) are close to each other (i.e. the difference is less than ca. 1 %), it can be concluded that carbon deposition does not take place under the pertinent operating conditions. The other significant result of the analyses, CO selectivity (S_{CO}), is defined as

$$S_{CO} = 100 \times \frac{y_{CO}}{y_{CO} + y_{CO_2}} \quad (3)$$

3 Results and Discussion

Experimental analysis of methane ATR in the microchannel reactor is conducted by changing one parameter in each run while keeping all others constant. Equilibrium methane conversion and CO selectivity are also calculated for each case using HSC Chemistry [36] via the Gibbs free energy minimization method. In all cases conversion below the equilibrium values is guaranteed by the choice of operating conditions such as contact times as short as 12.9 ms (Sect. 2.2) for the comparison of the parameter effects.

3.1 Effect of Residence Time

Catalytic ATR of hydrocarbons is reported to involve the occurrence of oxidation (TOX: $CH_4 + 2O_2 \rightarrow CO_2 + 2H_2O$, $\Delta H^o = -802.3$ kJ/mol), steam reforming (SR: $CH_4 + H_2O \leftrightharpoons CO + 3H_2$, $\Delta H^o = 206.2$ kJ/mol) and water–gas shift (WGS: $CO + H_2O \leftrightharpoons CO_2 + H_2$, $\Delta H^o = -41.2$ kJ/mol) reactions [37–39]. Combination of these key reactions seems to explain the findings given in Fig. 2 which shows the changes in methane conversion and CO selectivity with residence time (*RT* = 12.9 − 25.7 ms). Doubling the residence time leads to ~10 % increase in methane conversion (46.6 → 51.4 %). The continuous increase in methane consumption with residence time can be explained by the increased SR rate, which is a direct result of longer contact of the reactive stream with the catalyst layers. Since oxygen is depleted in all the runs in the parameter range, methane consumed during TOX is known by the stoichiometry of the reaction. This enables calculation of the amount of methane consumed during SR, hence the reforming rate, which exhibits a ~21 % increase with the doubling of the residence time.

The experimental CO selectivities are close to the equilibrium values. At residence times longer than 19 ms, however, actual selectivities turn out to be slightly higher than their counterparts calculated at equilibrium conditions (Fig. 2). A possible reason is that as CO production is taking place away from equilibrium, the selectivity is governed mostly by reaction kinetics [6, 40]. The slight increase in experimental selectivity can be attributed to the increase in the SR rate. Since the WGS reaction requires longer residence times (>ca. 45 ms [13]) to become significant, rate of CO formation remains higher than its consumption rate by WGS in the residence time range studied. Nevertheless, the outlet molar H_2/CO ratio range of 2.68−3.43 indicates that WGS still has some impact on the product distribution.

3.2 Effect of Temperature

The effect of reaction temperature on methane conversion and CO selectivity is presented in Fig. 3. Due to its positive effect on reaction kinetics, temperature is found to affect the product distribution significantly; experimental conversion increases from 12.8 to 46.6 % and experimental CO

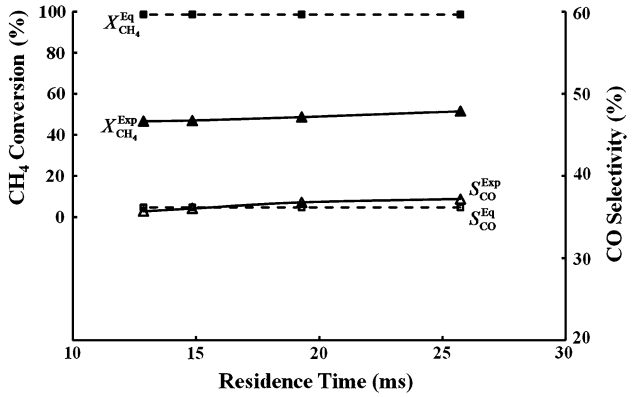

Fig. 2 Variation of experimental (Exp) and equilibrium (Eq) methane conversion and CO selectivity with residence time in the microchannel reactor (T = 650 °C, S/C = 3.0, O_2/C = 0.47)

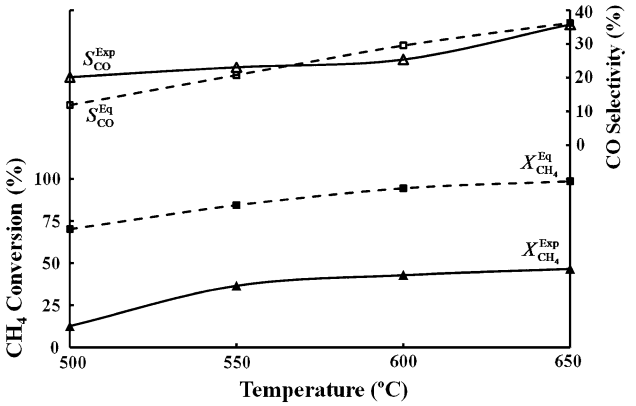

Fig. 3 Variation of experimental (Exp) and equilibrium (Eq) methane conversion and CO selectivity with reaction temperature in the microchannel reactor (RT = 12.9 ms, S/C = 3.0, O_2/C = 0.47)

selectivity increases from 20.1 to 35.7 % when the temperature is raised from 500 to 650 °C. Operation at 500 °C poses the only exception to full TOX conversion among the parametric runs (ca. 50 % instead of 100 %). As the reaction temperature falls below 570 °C, experimental CO selectivity exceeds equilibrium selectivity. In equilibrium-limited reaction systems like hydrocarbon reforming, reaction temperature determines whether the system is thermodynamically or kinetically controlled; and thermodynamic equilibrium is favored at elevated temperatures whereas the kinetic regime is dominant at lower temperatures [6, 40]. For the system under consideration, the temperature range in which product selectivity is controlled by reaction kinetics is found to be 500–570 °C.

3.3 Effect of S/C Ratio

The effect of molar S/C in the feed on CO selectivity and H_2/CO ratio in the product stream is shown in Fig. 4. The dependence of CO selectivity on the S/C ratio is weak. Conversion (not shown) increases merely by 10 % (from 41.5 to 46.6 %) and experimental CO selectivity shows a slight decrease ($\sim$8 %) as the ratio goes from 0 to 3.0. The H_2/CO ratio is most susceptible to changes in S/C whose variation determines the direction of the WGS reaction ($CO + H_2O \leftrightharpoons CO_2 + H_2$). Addition of extra steam should shift the WGS to the direction of CO_2 formation. However, at 650 °C the reverse WGS reaction is thermodynamically favored, which increases the CO concentration in the product mixture. The presence of CO_2 produced already by TOX also shifts the reaction to the left. As a result, H_2/CO ratios as low as 0.93 can be obtained. Referring to Fig. 4, $H_2/CO = 2.0$ is attainable with S/C $\approx$ 1.30. This finding, in conjunction with the results obtained in a temperature range (500–650 °C) lower than those involved in industrial reformers ($\geq \sim$1000 °C), has the strong implication that methane ATR carried out in catalytic microchannel reactors offers the promising option of producing syngas in a range of desired compositions with lower operational costs and fewer disruptions which are inevitable when working at elevated temperatures. The possibility of syngas production at lower temperatures is due to efficient heat transfer through the entire catalyst coating which is effectively utilized. This is one of the inherent drawbacks of packed-beds arising mainly from their poor heat transfer characteristics that are compensated by the supply of excessive external heat.

In addition to the benefits linked with improved heat transfer properties, syngas is produced without carbon formation even in the absence of steam in the feed (i.e. S/C = 0). This finding is supported by the facts that (a) the difference between Eqs (1) and (2) is found to be less than 1 %, (b) reactor effluent flow, which is periodically monitored, is observed to be pulse-free, indicating that the channel is not physically blocked by solid carbon deposition, and (c) no signs of deposition are detected after the

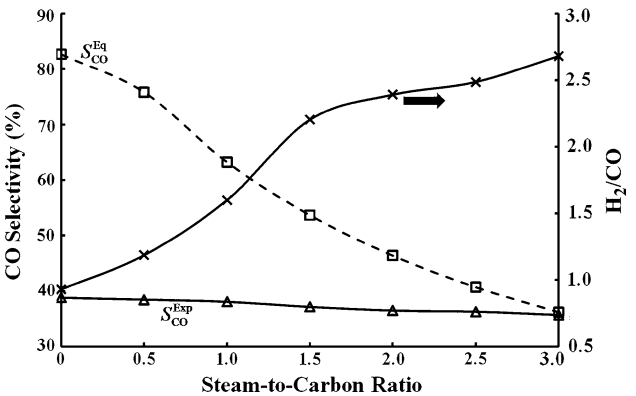

Fig. 4 Variation of experimental (Exp) and equilibrium (Eq) CO selectivity, and experimental H_2/CO ratio with the inlet molar S/C ratio in the microchannel reactor (RT = 12.9 ms, T = 650 °C, O_2/C = 0.47)

removal of the spent catalysts from the reactor. These outcomes are in alignment with the fact that millisecond-level residence times involved in microchannels are very short for carbon formation to occur. Moreover, recently reported results on non-oxidative steam reforming of methane to syngas run in microchannel reactor and catalyst configurations, and at operating conditions similar to those involved in the present work, do not indicate carbon deposition as observed through detailed SEM–EDX analyses [13].

3.4 Effect of O_2/C Ratio

The effect of molar O_2/C ratio in the feed on methane conversion and CO selectivity is given in Fig. 5. The $\sim$16 % increase (from 46.6 to 54.1 %) in conversion after the O_2/C ratio is changed from 0.47 to 0.63 is mainly the result of more methane converted during oxidation. As another remark, CO selectivity decreases by $\sim$11 % (from 35.7 to 32.1 %) with the O_2/C ratio since the production rate of CO_2 surpasses that of CO. This finding indicates that the effect of TOX becomes more visible when feed becomes rich with O_2. It is also worth noting that the rate of decrease in experimental selectivity in the O_2/C = 0.47–0.54 range is less than that observed in the O_2/C range of 0.54–0.63. This result points to the possibility of direct partial oxidation of methane to syngas (POX: $CH_4 + 0.5O_2 \rightarrow CO + 2H_2$, $\Delta H^o = -35.7$ kJ/mol) which is reported to be favored at residence times in the order of milliseconds and at lower oxygen quantities in the reactive mixture [41]. The co-existence of POX with TOX leads to lower quantities of CO_2 product. However, as the O_2 content is increased further, the dominance of TOX gets to be more notable as verified by the faster rate of decrease in experimental CO selectivity.

The order between the experimental and equilibrium CO selectivities is found to change in the O_2/C ratio range studied. Recalling that when the O_2/C ratio is equal to 0.47, the threshold temperature is 570 °C for transition from the kinetic to the thermodynamic regime (Fig. 5), it may be said that at higher temperatures the actual selectivity should be less than the equilibrium selectivity unless the TOX and SR reaction mechanisms are altered by some other parameter. However, at 650 °C, the temperature at which the O_2/C parameter is investigated, the actual selectivity is still measured to be higher in almost the entire range of O_2/C ratios (0.47–0.63), possibly due to the alteration of reaction paths by increased O_2 in the feed [40].

3.5 Effect of Catalyst Configuration

In addition to the effect of operating parameters given above, the impact of microchannel catalyst configuration

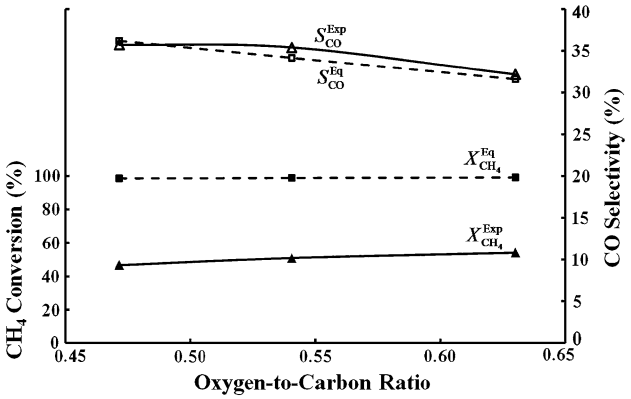

Fig. 5 Variation of experimental (Exp) and equilibrium (Eq) methane conversion and CO selectivity with the inlet molar O_2/C ratio in the microchannel reactor (RT = 12.9 ms, T = 650 °C, S/C = 3.0)

on methane conversion and CO selectivity is also considered. For this purpose, the performance of the present configuration with monometallic 0.2 wt% Pt/δ-Al_2O_3 and 2 wt% Rh/δ-Al_2O_3 catalyst plates facing each other in the microchannel (see Sect. 2.1, Fig. 1a, b), is compared with that of another configuration described by two bimetallic 0.2 %Pt-2 %Rh/δ-Al_2O_3 plates that are placed into the steel housing as shown in Fig. 1a, b. Both microchannel configurations involved almost the same amount of Rh metal (2.1×10^{-4} g), whereas the amount of Pt metal (3.1×10^{-5} g) was slightly above that coated in the bimetallic plate (2.1×10^{-5} g) [34]. Both configurations are tested in the identical reaction system and under reaction conditions described in Sect. 2.2 and in Table 1. The catalyst synthesis and coating procedures given in Sect. 2.1 are also followed for obtaining the bimetallic Pt–Rh coated catalyst, which is prepared by the sequential addition of Rh (2 % by weight) and Pt (0.2 %) metals to the δ-Al_2O_3 support by the incipient-to-wetness impregnation technique, whose details are described elsewhere [34].

A comparsion of the two microchannel catalyst types are given in Table 2. It can be observed that the bimetallic catalyst configuration [34] gives higher methane conversions than the one with two monometallic catalysts in the entire range of operating conditions studied. These findings can be discussed in terms of a possible interaction between the adjacent Pt and Rh sites to generate a synergetic effect that can lead to higher reaction rates and conversions, as also reported in studies involving similar bimetallic catalyst systems [34, 42]. The bimetallic microchannel is better than the present configuration also in terms of CO selectivity. The mentioned benefits of the bimetallic system become more visible when the residence time is increased from 12.9 to 25.7 ms, which means that the synergetic impact turns out to be more significant due to the increased contact/interaction of the reactive flow with the catalyst: at

Table 2 Effects of microchannel catalyst configuration on methane conversion and CO selectivity

	Monometallic Pt and Rh coated microchannel (Present work)		Bimetallic Pt-Rh coated microchannel [34]	
	X_{CH_4} (%)	S_{CO} (%)	X_{CH_4} (%)	S_{CO} (%)
T (°C)				
500	12.76	20.11	31.03	7.34
550	36.65	23.05	38.93	18.43
600	42.92	25.38	44.49	36.61
650	46.58	35.70	51.21	41.89
S/C (mol/mol)				
0	42.56	38.78	45.46	48.94
0.5	41.49	38.44	44.23	43.00
1.0	42.39	38.06	44.89	42.92
1.5	43.15	37.14	47.72	42.45
2.0	46.16	36.49	49.08	42.39
2.5	46.31	36.28	50.14	42.20
3.0	46.58	35.70	51.21	41.89
O_2/C (mol/mol)				
0.47	46.58	35.70	51.21	41.89
0.54	50.87	35.39	52.25	40.90
0.63	54.11	32.14	57.47	40.29
RT (ms)				
12.9	46.58	35.70	51.21	41.89
14.8	45.94	36.04	54.06	48.21
19.3	48.57	36.77	56.89	48.74
25.7	51.40	37.18	61.71	49.41

25.7 ms, differences in conversion and selectivity are calculated to be 20 and 33 %, respectively (Table 2). The positive trend provided by the bimetallic system is disturbed only at 500 and 550 °C, at which temperature window Pt–Rh is found to give lower selectivities due to the possible occurence of WGS driven by the same synergy. It is also worth noting that the response trends against changes in the parameter values are similar for both configurations.

4 Conclusions

Experimental analysis of methane ATR that involves parametric variations of the residence time, reaction temperature, and inlet S/C and O_2/C molar ratios is carried out in a microchannel reactor involving alumina supported Pt and Rh catalysts coated on the opposite walls of the channel. The largest changes in methane conversion (from 12.8 to 46.6 %) and in CO selectivity (from 20.1 to 35.7 %) are obtained by raising the temperature from 500 to 650 °C. While ~10 % increase is observed in methane conversion with doubling of the residence time, selectivity is improved only by 4 %. Increase in the O_2/C ratio leads to higher CH_4 conversions due to the increased extent of oxidation, but CO selectivity is reduced due to CO_2 production. The product H_2/CO ratio is found to be highly susceptible to changes in the feed S/C ratio, which can conveniently be manipulated between 0 and 3.0 to adjust the syngas composition between 0.93 and 2.68. This outcome shows the possibility of producing Fischer–Tropsch grade syngas (H_2/CO ≈ 2.0) in microchannel reactors at 650 °C which is considerably lower than the temperatures involved in industrial autothermal reformers (≥ ~1000 °C). Further improvement of CO selectivity, i.e. reduction of H_2/CO ratio in syngas composition, is possible by replacing the monometallic Pt and Rh catalyst coatings with those utilizing bimetallic Pt–Rh coatings in the microchannel reactor.

Acknowledgments Financial support is provided by TUBITAK through project MAG-108M509 and by Bogazici University Research Fund through project BAP-6349. Ahmet K. Avci acknowledges TUBA-GEBIP program.

References

1. Aasberg-Petersen K, Bak Hansen JH, Christensen TS, Dybkjaer I, Seier Christensen S, Stub Nielsen C, Winter Madsen SEL, Rostrup-Nielsen JR (2001) Appl Catal A 221:379–387
2. Steynberg AP (2004) In: Steynberg AP, Dry M (eds) Fischer-Tropsch technology. Elsevier, UK
3. Tan O, Masalaci E, Onsan ZI, Avci AK (2008) Int J Hydrogen Energy 33:5516–5526
4. Orucu E, Karakaya M, Avci AK, Onsan ZI (2005) J Chem Technol Biotechnol 80:1103–1110
5. Spath PL, Dayton DC (2003) Technical Report NREL/TP-510-34929, National Renewable Energy Laboratory
6. Dissanayake D, Rosynek MP, Kharas KCC, Lunsford JH (1991) J Catal 132:117–127
7. Mukainakano Y, Li B, Kado S, Miyazawa T, Okumura K, Miyao T, Naito S, Kunimori K, Tomishige K (2007) Appl Catal A 318:252–264
8. Tomishige K (2007) J Jpn Pet Inst 50:287–298
9. Tomishige K, Kanazawa S, Suzuki K, Asadullah M, Sato M, Ikushima K, Kunimori K (2002) Appl Catal A 233:35–44
10. Li B, Maruyama K, Nurunnabi M, Kunimori K, Tomishige K (2004) Appl Catal A 275:157–172
11. Rostrup-Nielsen JR (1984) In: Anderson JR, Boudart M (eds) Catalysis, science & technology. Springer-Verlag, Berlin
12. Rostrup-Nielsen JR, Sehested J, Nørskov JK (2002) Adv Catal 47:65–139
13. Karakaya M, Keskin S, Avci AK (2012) Appl Catal A 411–412:114–122
14. Wang Y, Chin YH, Rozmiarek RT, Johnson BR, Gao Y, Watson J, Tonkovich AYL, Vander Wiel DP (2004) Catal Today 98:575–581
15. Onsan ZI, Avci AK (2011) In: Shekhawat D, Spivey JJ, Berry DA (eds) Fuel cells: technologies for fuel processing. Elsevier, Amsterdam
16. Avci AK, Trimm DL, Karakaya M (2010) Catal Today 155:66–74

17. Karakaya M, Avci AK (2010) Int J Hydrogen Energy 35:2305–2316
18. Karakaya M, Avci AK, Aksoylu AE, Onsan ZI (2009) Catal Today 139:312–321
19. Hosukoglu MI, Karakaya M, Avci AK (2012) Ind Eng Chem Res 51:8913–8921
20. Gumuslu G, Avci AK (2012) AIChE J 58:227–235
21. Karakaya M, Avci AK (2011) Int J Hydrogen Energy 36:6569–6577
22. Kolb G, Hessel V (2004) Chem Eng J 98:1–38
23. Tonkovich ALY, Yang B, Perry ST, Fitzgerald SP, Wang Y (2007) Catal Today 120:21–29
24. Fichtner M, Mayer J, Wolf D, Schubert K (2001) Ind Eng Chem Res 40:3475–3483
25. Younes-Metzler O, Svagin J, Jensen S, Christensen CH, Hansen O, Quaade U (2005) Appl Catal A 284:5–10
26. Enger BC, Walmsley J, Bjørgum E, Lødeng R, Pfeifer P, Schubert K, Holmen A, Venvik HJ (2008) Chem Eng J 144:489–501
27. Makarshin LL, Andreev DV, Gribovskyi AG, Parmon VN (2011) Chem Eng J 178:276–281
28. Bae JM, Ahmed S, Kumar R, Doss E (2005) J Power Sources 139:91–95
29. Chen G, Li S, Yuan Q (2007) Catal Today 120:63–70
30. Peela NR, Kunzru D (2011) Int J Hydrogen Energy 36:3384–3396
31. Johnson BR, Canfield NL, Tran DN, Dagle RA, Li XS, Holladay JD, Wang Y (2007) Catal Today 120:54–62
32. Zhai X, Ding S, Liu Z, Jin Y, Cheng Y (2011) Int J Hydrogen Energy 36:482–489
33. Simsek E, Avci AK, Onsan ZI (2011) Catal Today 178:157–163
34. Simsek E, Karakaya M, Avci AK, Onsan ZI (2013) Int J Hydrogen Energy 38:870–878
35. Avci AK, Trimm DL, Aksoylu AE, Onsan ZI (2004) Appl Catal A 258:235–240
36. Roine A, Outokumpu HSC Chemistry 6.1, Pori, Finland
37. Trimm DL, Adesina AA, Praharso, Cant NW (2004) Catal Today 93–95:17–22
38. Tsolakis A, Golunski SE (2006) Chem Eng J 117:131–136
39. Tsolakis A, Megaritis A, Golunski SE (2005) Energ Fuels 19:744–752
40. Choudhary VR, Rajput AM, Prabhakar B (1993) J Catal 139:326–328
41. Hickman DA, Schmidt LD (1993) Science 259:343–346
42. Avci AK, Trimm DL, Aksoylu AE, Onsan ZI (2003) Catal Lett 88:17–22